UDC 519.6+51-74::628.395

MEMBRANE FOULING CHARACTERISTICS DURING FILTRATION AND TRANSPORT PROCESSES IN A CYLINDRICAL POROUS FILTER

Ravshanov N., Boborakhimov B.I., *Berdiyorov Sh.Sh.

*berdiyorovsh@gmail.com

Digital technologies and artificial intelligence development research institute,
17A, Buz-2, Tashkent, 100125 Uzbekistan.

This study presents a mathematical and numerical model for filtration flow, solute transport, adsorption, and membrane fouling in a cylindrical porous filter. The model combines axisymmetric Brinkman–Darcy flow equations with advection–diffusion–reaction equations, Langmuir adsorption, and the linear driving force (LDF) model. It also considers porosity changes, particle deposition, cake formation, osmotic pressure, and membrane resistance growth. A finite difference scheme with CFL-based stability control is used for simulations. Results show that adsorption and particle deposition significantly reduce porosity and membrane permeability, leading to increased hydraulic resistance and flux decline. The model provides a useful framework for predicting fouling dynamics and optimizing porous filtration systems.

Keywords: cylindrical porous filter, membrane fouling, Brinkman–Darcy model, advection–diffusion–reaction equations, adsorption kinetics, Langmuir isotherm, concentration polarization, osmotic pressure, cake layer formation, porous media transport, finite difference method, filtration processes.

Citation: Ravshanov N., Boborakhimov B.I., Berdiyorov Sh.Sh. 2026. Membrane fouling characteristics during filtration and transport processes in a cylindrical porous filter. *Problems of Computational and Applied Mathematics.* 3(73): 104-124.

DOI: https://doi.org/10.71310/pcam.3_73.2026.08

1 Introduction

The study of filtration and transport phenomena in porous media is important in many industrial and environmental fields, such as water treatment, chemical treatment, and filtration systems. The behavior of fluids in these systems is strongly influenced by their physical properties, which in turn affects flow dynamics and mass transfer processes.

The main physical properties of liquids include viscosity, density, and diffusion coefficients. Viscosity determines flow resistance and significantly affects the filtration rate and pressure loss in porous structures. Changes in density can alter the stability and distribution of the flow, which is especially noticeable in systems where gravitational or buoyancy forces act. Diffusion coefficients regulate the movement of substances dissolved in a liquid and play a crucial role in transport efficiency.

In cylindrical porous filters, both the geometry of the system and the properties of the porous medium form complex flow patterns. The interaction between fluid properties and the porous matrix affects velocity fields, pressure distributions, and concentration profiles. Understanding these effects is essential for designing and improving the performance of filtration systems.

Although filtration processes have been extensively studied, the influence of fluid physical properties in cylindrical porous systems remains a significant research topic. A deeper

understanding of these effects will help develop more efficient filtration technologies and improve the control of transport processes in porous media.

A mathematical and computational model describing the filtration of liquid solutions in a cylindrical porous filter was developed in [1]. Its structure is based on the Brinkman-Darcy equations for describing fluid flow in a porous medium, and the porosity and permeability are related to the Kozeni-Karman equation. The transport of dissolved substances is modeled using an advection-diffusion-reaction scheme, supplemented by the kinetics of the linear driving force (LDF) and the adsorption isotherm of Langmuir. Furthermore, the model features a colmatation mechanism that prevents the accumulation of particles and, consequently, a time-dependent decrease in filter porosity. Based on the combined gradient method, a finite-difference numerical scheme containing an iterative pressure correction procedure has been implemented while maintaining stability under the Courant-Friedrichs-Lewy condition.

The study [2] examines the digital modeling of flow during the filtration and transport of dissolved components in a cylindrical porous medium. The mathematical expression is based on the axially symmetric Brinkman-Darcy equations describing hydrodynamics, as well as a system of equations for calculating convective-diffusion transport - adsorption in a solid matrix. undefined The numerical solution is carried out using the following formula: the finite volume method, which guarantees that the conservation laws are met under each control. A computational algorithm, velocities, and component concentrations have been developed to determine the pressure distribution. The influence of the porous structure on the parameters and characteristics of the adsorption kinetics of the filtration process was studied.

In work [3] proposes an analytical solution to the filtration problem in a sandwich-type collector system, including the determination of pressure distribution in the low-permeability layer. A new generalized formula for managing well galleries has also been proposed. The developed mathematical framework allows for the design of layout schemes and the capacity of vertical drainage wells, the prevention of flooding in irrigated and non-irrigated areas, the protection of groundwater from pollution sources, and the proposal of practical solutions for the isolation of already polluted zones.

In work [4], a mathematical model and an efficient numerical algorithm were developed for a comprehensive study of the technological process of filtration of liquids and ionized solutions. The proposed model takes into account changes in the filtration rate, changes in the suspension concentration in the column and at the outlet, the formation of a sediment layer on the filter surface, the accumulation of gel particles in the filter pores, pressure increases in both the column and the sediment layer, and other physical and mechanical properties of the filtered liquid. Computational experiments were conducted, and the results obtained were presented graphically to analyze the operating modes of the filtration system under the influence of various suspension properties and external factors and to support decision-making.

In paper [5] examines the mathematical modeling of plane-parallel isotropic liquid filtration and emphasizes its importance for the stability of hydraulic structures. Filtration can lead to water loss from reservoirs, reverse pressure effects, and internal hydrodynamic forces. In isotropic media, permeability is assumed to be equal in all directions, and under the hydraulic pressure of the dam, water flows from the upstream to the downstream. The upper limit of filtration is determined by the depression curve, which can reach the lower slope and cause a residual pressure flow along its surface. This process can transport soil

particles (suffusion), increase soil permeability, and potentially destabilize the downstream slope, ultimately threatening the safety of the dam.

In the study, along with formulas for determining fluid flow in the well, the regularities for regulating pressure distribution under conditions of direct radial flow were considered, taking into account horizontal and vertical directions [6].

The proposed model describes two-phase (oil-water) filtration based on the mass balance equations for each phase and Darcy's law, which allows for the study of injection and operation processes in the section of the wellbore and the surrounding formation. The modeling results emphasize the influence of crack diameter on pressure distribution and water saturation. These findings allow for the determination of optimal operating modes for injection wells and the prediction of water breakthrough rates and the development rate of corresponding wells using numerical methods with low calculation errors [7].

In the study of fluid dynamics and porous media, nonlinear fluid filtration in two-layer systems is a significant problem that requires a solid mathematical basis for precise description and analysis. This article presents a multi-parameter mathematical model aimed at determining the complexity of filtration processes in a heterogeneous medium, focusing specifically on the two-layer medium. The research is aimed at the development and numerical solution of nonlinear filtration problems for structural and non-structural fluids in multilayer layers with different properties of hydrodynamically bound. The proposed models and computational algorithms were confirmed using a set of hypothetical data and demonstrated their applicability and effectiveness [8].

This research aims to develop a mathematical model for the nonlinear filtration of fluids formed in a layered medium. In the analysis, the flow velocity between layers is studied as a function of the properties of the layer and the liquid. Furthermore, numerical algorithms were developed to support computational experiments and validate the proposed model [9].

This article develops a mathematical model describing fluid filtration in underground layers under electricity generation conditions. It studies both Newtonian fluids and abnormally structured fluids as media that undergo filtration. The computational system is based on both direct and simplified differential approaches, as well as iterative methods. A numerical study is also conducted, allowing for the assessment of intercollector flow velocities and the determination of fracture boundary locations, taking into account the dynamics of formation evolution [10].

Recently, the biological extraction of acrylonitrile (AN) from exhaust gas streams has attracted significant interest due to its high efficiency. In this study, the main focus is on developing a model for the elimination of AN using a biofilter. The model was confirmed by experimental data obtained from a biofilter column filled with backyard waste compost, crushed plastic materials, and concentrated urban activated clay. Initially, the kinetics of acrylonitrile biodegradation were studied, followed by the derivation of control equations for both the biofilm and gas phases under stable conditions and at constant temperatures. The unknown parameters of the model were evaluated using the least-squares optimization approach in conjunction with numerical solutions to the MATLAB-based system equations [11].

The anomalous filtration of a liquid in a porous medium is described using differential equations containing fractional derivatives in the Caputo sense. In this work, the filtration process in a bounded homogeneous layer was investigated and numerically solved, paying special attention to the influence of anomalous influences on the filtration state. The results show that in the pressure-dependent relaxation term, a decrease in the fractional

order decreases the pressure distribution to a certain distance from the layer boundary, after which it begins to increase. Conversely, a decrease in the fractional order of the term associated with the filtration rate has the opposite effect. Overall, the filtration dynamics change significantly as fractional orders decrease [12].

In this study, a model of anomalous filtration and dissolved matter transport in a two-zone medium with a ribbon source was developed and numerically solved. In one zone, transport is governed by anomalous convective-diffusion dynamics, while in another zone, it is governed by pure diffusion. The study will further investigate how anomalous impacts affect the overall transport behavior of the system [13].

In [14], the effect of a uniform magnetic field on a stable, incompressible laminar flow of a non-Newtonian Casson fluid over an elongating surface immersed in a porous medium is considered under conditions of local thermal imbalance (LTNE). Separate temperature graphs are adopted for the liquid and solid phases. Using appropriate similarity transformations, the governing partial differential equations are converted into ordinary differential equations, which are then numerically solved using the fourth-order Runge-Kutta method and the throwing method.

In the study [15], a mathematical model of fluid filtration in a multilayer porous cylinder was developed using the continuity equation in conjunction with Darcy's law. The cylinder consists of seven polypropylene fiber layers, each of which has a separate filtering function. Filter contamination is modeled using a single-component suspension approach, which includes empirical parameters that account for changes in sediment porosity, adsorption-desorption processes, permeability, and viscosity. To eliminate the complexity of the computational process, the authors propose using parallel computations alongside distributed finite element methods on high-performance computing platforms. This strategy allows for effective simulation and lays the foundation for the future implementation of hydrodynamic filtration models.

2 Problem formulation

Below are the equations for a cylindrical porous filter.

Equations for hydraulics (Brinkman-Darcy):

$$\frac{1}{r}\frac{\partial(ru_r)}{\partial r}+\frac{\partial u_z}{\partial z}=0, \tag{1}$$

$$-\frac{\mu}{\varkappa(\varepsilon)}u_r+\mu\left(\frac{1}{r}\frac{\partial}{\partial r}\left(r\frac{\partial u_r}{\partial r}\right)+\frac{\partial^2 u_r}{\partial z^2}-\frac{u_r}{r^2}\right)-\frac{\partial p}{\partial r}=0, \tag{2}$$

$$-\frac{\mu}{\varkappa(\varepsilon)}u_z+\mu\left(\frac{1}{r}\frac{\partial}{\partial r}\left(r\frac{\partial u_z}{\partial r}\right)+\frac{\partial^2 u_z}{\partial z^2}\right)-\frac{\partial p}{\partial z}=0, \tag{3}$$

$$\varkappa(\varepsilon)=\frac{\varepsilon^3 d_f^2}{180(1-\varepsilon)^2}. \tag{4}$$

Here: r is the radial coordinate $[m]$, z is the vertical coordinate $[m]$, u_r is the radial velocity component $[m/s]$, u_z is the vertical velocity component $[m/s]$, the angular coordinate is taken as zero due to symmetry, $\mu=\mu(T)$ denotes the dynamic viscosity $[Pa{\cdot}s]$, $\varkappa(\varepsilon)$ is the permeability $[m^2]$, p is the pressure $[Pa]$, ε is the porosity, $(0<\varepsilon<1)$, d_f – is the filter particle diameter $[m]$.

Here, (1) is the conservation of mass equation and represents the uncompressibility of water. It ensures the balance of incoming and outgoing volumes, ensuring mass preservation regardless of the internal pressure in the filter. Equation (2) corresponds to the

radial balance of momentum, which describes the radial velocity under the influence of the pressure gradient and the resistance of the porous medium. When there is a pressure difference between the center and the wall, the fluid moves radially, and the resistance of the pores slows down this movement. The next equation controls the axial pulse, which controls the flow in the main direction from top to bottom. Here, the pressure difference drives the motion, while the viscosity and porosity resistance reduce the flow rate. As a result, the flow rate depends on the applied pressure gradient. The last equation is the Kozeni-Karman relation, which relates the internal structure of the filter, in particular its porosity, to its permeability. A more porous or coarse-grained medium allows fluid to pass through more easily and increases overall permeability.

For liquids, the viscosity is approximated as

$$\mu = a \cdot 10^{\frac{b}{T-c}}. \tag{5}$$

Where again T is absolute temperature and a, b and c are experimentally determined constants. For water, using the values $a = 2.414 \times 10^{-5}$ N $\cdot$ s/m^2, $b = 247.8K$, and $c = 140K$ results in less than 2.5 percent error in viscosity in the temperature range of 0°C to 370°C (Touloukian et al.,1975).

Dynamic viscosity of liquid water from $kg/(m \cdot s)$ to 50°C.

Table 1 Temperature dependence of dynamic viscosity

Temperature (°C)	Dynamic viscosity (Pa·s)	Temperature (°C)	Dynamic viscosity (Pa·s)
0	0.001792	26	0.000871
1	0.001731	27	0.000852
2	0.001674	28	0.000833
3	0.001620	29	0.000815
4	0.001569	30	0.000798
5	0.001520	31	0.000781
6	0.001473	32	0.000765
7	0.001429	33	0.000749
8	0.001386	34	0.000734
9	0.001346	35	0.000720
10	0.001308	36	0.000705
11	0.001271	37	0.000692
12	0.001236	38	0.000678
13	0.001202	39	0.000666
14	0.001170	40	0.000653
15	0.001139	41	0.000641
16	0.001109	42	0.000629
17	0.001081	43	0.000618
18	0.001054	44	0.000607
19	0.001028	45	0.000596
20	0.001003	46	0.000586
21	0.000979	47	0.000576
22	0.000955	48	0.000566
23	0.000933	49	0.000556
24	0.000911	50	0.000547
25	0.000891		

For substance transport (for each $i = 1, \ldots, N$), the following equations (6)-(9) are expressed:

For substance transport (for each $i = 1, \ldots, N$), the following equations (6) – (9) are expressed:

$$\frac{\partial (\varepsilon c_i)}{\partial t} + \nabla \cdot (u c_i) = \nabla \cdot (\varepsilon D_i \nabla c_i) - r_i^{bulk} - a_s r_i^{surf}, \tag{6}$$

$$\frac{\partial q_i}{\partial t} = k_{f,i}(q_i^* - q_i), \tag{7}$$

$$q_i^* = \frac{q_{i,\max} b_i c_i}{1 + \sum_{j=1}^{N} b_j c_j}, \tag{8}$$

$$r_{i,surf} = \rho_s \frac{\partial q_i}{\partial t}. \tag{9}$$

Where: t – time $[s]$, N – number of components, c_i – concentration of the i-th component in water $[mol/m^3$ or $kg/m^3]$, $D_{i,\text{eff}}$ – effective diffusion coefficient $[m^2/s]$, $r_{i,\text{bulk}}$ – bulk reaction rate in solution $[mol/(m^3 \cdot s)]$, a_s – surface area of per unit volume $[m^2/m^3]$, $r_{i,\text{surf}}$ – surface loss rate $[mol/(m^2 \cdot s)]$,q_i – capture quantity in the solid phase $[mol/kg]$, $k_{f,i}$ – LDF(linear driving force) kinetic coefficient $[1/s]$, q_i^* – equilibrium adsorption quantity $[mol/kg]$, $q_{i,\max}$ – maximum adsorption capacity $[mol/kg]$, b_i – Langmuir affinity coefficient $[m^3/mol]$, ρ_s – density of adsorbent particles $[kg/m^3]$.

Equation (6) is the advection-diffusion-reaction (ADR) equation, which describes how the concentration of each pollutant in the water changes. It accounts for changes due to transport by flow (advection), dispersion by diffusion, elimination by reaction, and reduction by adsorption. This equation is used to evaluate the quality of filtered water at the outlet. Equation (7) represents a linear kinetic model of adsorption, which determines the rate of contaminant retention by filter particles. With a large number of adsorption sites, absorption is fast, but as the particles become saturated, the adsorption rate decreases. The next equation is the Langmuir isotherm, which describes the adsorption state under limited surface conditions. Due to limited adsorption sites, pollutants compete for free space, and filtration efficiency gradually decreases over time. The latter equation describes the rate of change of the surface load, shows how adsorption in the solid phase develops and reduces the concentration in the liquid phase. This term relates the transfer of pollutants between the liquid and solid phases through the process of adsorption.

The colmatation equations (10)-(11) defined as follows:

$$\begin{aligned} &\frac{\partial (\varepsilon c_p)}{\partial t} + \frac{1}{r}\frac{\partial}{\partial r}(r c_p u_r) + \frac{\partial}{\partial z}(c_p u_z) = \\ &= \frac{1}{r}\frac{\partial}{\partial r}\left(r \varepsilon D_p \frac{\partial c_p}{\partial r}\right) + \frac{\partial}{\partial z}\left(\varepsilon D_p \frac{\partial c_p}{\partial z}\right) - k_{\text{dep}} c_p, \end{aligned} \tag{10}$$

$$\frac{\partial \varepsilon}{\partial t} = -\frac{\nu_{\text{dep}}}{\rho_{\text{dep}}} k_{\text{dep}} c_p. \tag{11}$$

Where: c_p – concentration of particulate matter in water $[\text{kg/m}^3]$, D_p – diffucion coefficient of particles $[\text{m}^2/\text{s}]$, k_{dep} – deposition coefficient $[1/\text{s}]$, ν_{dep} – volume fraction of deposition [–], ρ_{dep} – density of settled particles $[\text{kg/m}^3]$.

In this situation, larger particles such as sand and clay clog the pores, leading to a reduction in the filter's permeability. Consequently, the flow rate gradually decreases over time.

$$J_i = (1 - \sigma_i)\, c_{i,\text{avg}}\, J_v - P_{s,i}\, \Delta c_i, \tag{12}$$

$$J_v = \frac{\Delta p}{\mu(R_m + R_c)}, \tag{13}$$

$$R_c = \alpha_c \delta_c, \tag{14}$$

$$\frac{\partial \delta_c}{\partial t} = \frac{J_v\, c_{p,m}}{\rho_c}. \tag{15}$$

Here: G_{in} – inlet surface (from above, $z = 0$), G_{out} – outlet surface (from below, $z = H$), J_v – volumetric flow through the membrane (permeat flux) $[m/\text{s}]$, L_p – membrane hydraulic permeability $[m/(Pa{\cdot}s)]$, Δp – transmembrane pressure difference $[Pa]$, σ_i – reflection coefficient [-], π_i – osmotic pressure $[Pa]$, J_i – membrane flow of the i-th component $[mol/(m^2{\cdot}s)]$, $c_{i,\text{avg}}$ – average concentration near the membrane $[mol/m^3]$, $P_{s,i}$ – salt permeability $[m/s]$, $\partial/\partial n$ – normal derivative operator (at the membrane level), R_m – internal membrane resistance $[1/m]$, – cake resistance $[1/m]$, α_c – specific cake resistance $[m/kg]$, $\delta_c(r, z, t)$ – cake thickness $[m]$, $c_{p,m}$ – particle concentration on the membrane $[kg/m^3]$, ρ_c – cake density $[kg/m^3]$.

Boundary and initial conditions

The computational domain is an axisymmetric cylindrical domain

$$\Omega = \{(r, z) : 0 \leqslant r \leqslant R,\ 0 \leqslant z \leqslant H\}. \tag{16}$$

To close the system of equations (1)-(8), the following boundary and initial conditions are specified.

At the filter inlet ($z = 0$), a uniform axial flow of liquid and known concentrations of components are set:

$$\begin{cases} u_z(r, 0) = u_{in}, \\ u_r(r, 0) = 0, \\ c_i(r, 0) = c_{i,in},\ i = 1, \ldots, N. \end{cases} \tag{17}$$

Neumann's condition is used for pressure:

$$\left.\frac{\partial p}{\partial z}\right|_{z=0} = 0. \tag{18}$$

At the filter outlet ($z = H$), a fixed pressure is set, and for the remaining values, the conditions of zero longitudinal gradient are met:

$$\begin{cases} p(r, H) = p_{out}, \\ \left.\dfrac{\partial u_z}{\partial z}\right|_{z=H} = J_v, \\ \left.\dfrac{\partial u_r}{\partial z}\right|_{z=H} = 0, \\ \left.\dfrac{\partial c_i}{\partial z}\right|_{z=H} = 0,\ i = 1, \ldots, N. \end{cases} \tag{19}$$

Axis of symmetry ($r = 0$): Due to the axisymmetric nature of the solution, the following conditions are satisfied:

$$\begin{cases} u_r(0,z) = 0, \\ \left.\dfrac{\partial u_z}{\partial r}\right|_{r=0} = 0, \\ \left.\dfrac{\partial p}{\partial r}\right|_{r=0} = 0, \\ \left.\dfrac{\partial c_i}{\partial r}\right|_{r=0} = 0,\ i = 1, \ldots, N. \end{cases} \tag{20}$$

Side surface of the filter ($r = R$): On the side wall of the filter, the adhesion conditions for the velocity and the absence of diffusion flow of substances are set:

$$\begin{cases} u_r(R,z) = 0, \\ u_z(R,z) = 0, \\ \left.\dfrac{\partial p}{\partial r}\right|_{r=0} = 0, \\ \left.\dfrac{\partial c_i}{\partial r}\right|_{r=R} = 0,\ \ i = 1, \ldots, N. \end{cases} \tag{21}$$

Membrane level (if applicable, G_m) boundary conditions

$$\begin{cases} u_n = J_v, J_v = L_p\left(\Delta p - \sum\limits_{i=1}^{N} \sigma_i \Delta\pi_i\right), \\ J_v = \dfrac{\Delta p}{\mu(R_m + R_c)}, \\ -\varepsilon D_{i,eff}\dfrac{\partial c_i}{\partial n} + u_n c_i = J_i, i = 1, \ldots, N, \\ J_i = (1-\sigma_i) J_v c_{i,\mathrm{avg}} - P_{s,i}\Delta c_i,. \end{cases} \tag{22}$$

Initial conditions ($t = 0$):

For a non-stationary problem, the initial conditions are given in the form:

$$u_r(r,z,0) = u_{r,0}(r,z),\ u_z(r,z,0) = u_{z,0}(r,z),\ p(r,z,0) = p_0(r,z), \tag{23}$$

$$\begin{cases} c_i(r,z,0) = c_{i,0}, \\ q_i(r,z,0) = 0,\ \ i = 1, \ldots, N, \\ \varepsilon(r,z,0) = \varepsilon_0(r,z), \delta_c(r,z,0) = 0, \\ R_c(r,z,0) = 0, J_v(r,0) = J_{v,0}. \end{cases} \tag{24}$$

At the initial stage, the filter is considered free of sediment, without particle accumulation, and adsorptionally unsaturated. As a result, both the cake layer thickness and the additional hydraulic resistance are taken to be zero. The initial velocity and pressure distribution is determined by solving the hydrodynamic equations stabilized under membrane non-contamination conditions. Accordingly, the velocity and pressure fields are initialized using a stationary hydrodynamic solution.

3 Solution of the problem

Obtaining exact analytical solutions to the above equations is very difficult and often impractical. Therefore, numerical methods are used when approximating solutions. Among them, the finite difference method is one of the most effective. The process of solving with this method usually includes the following steps:

Grids and designations are entered as follows:

Spatial nodes – $r_i = i\Delta r, i = 0, \ldots, N_r$; $z_j = j\Delta z, j = 0, \ldots, N_z$.

Time - $t^n = n\Delta t, n = 0, 1, 2, \ldots$.

Discrete fields - $p^n_{i,j}$, $u^n_{r,i,j}$, $u^n_{z,i,j}$.

Concentration for each component - $k = 1, \ldots, N$, concentration - $c^n_{k,i,j}$, adsorption - $q^n_{k,i,j}$.

Partion concentration: $c^n_{p,i,j}$; porosity: $\varepsilon^n_{i,j}$; membrane layer: $\delta^n_{c,i}$ (if present, at $j = N_z$), $\varkappa^n_{i,j}$ – permeability (Kozeny–Carman).

Auxiliary network nodes are entered as follows:

$$r_{i+\frac{1}{2}} = r_i + \frac{\Delta r}{2}, \;\; u^n_{r,i+\frac{1}{2},j} = \frac{u^n_{r,i+1,j} + u^n_{r,i,j}}{2}.$$

Auxiliary differential operators (central differences) are defined as follows:

Central gradient operator diagram

$$\left(\frac{\partial \varphi}{\partial r}\right)^n_{i,j} = \frac{\varphi^n_{i+1,j} - \varphi^n_{i-1,j}}{2\Delta r}, \left(\frac{\partial \varphi}{\partial z}\right)^n_{i,j} = \frac{\varphi^n_{i,j+1} - \varphi^n_{i,j-1}}{2\Delta z}.$$

Cylindrical Laplace operator diagram

$$(\nabla^2 \varphi)^n_{i,j} = \frac{1}{r_i}\frac{\varphi^n_{i+1,j} - \varphi^n_{i-1,j}}{2\Delta r} + \frac{\varphi^n_{i+1,j} - 2\varphi^n_{i,j} + \varphi^n_{i-1,j}}{\Delta r^2} + \frac{\varphi^n_{i,j+1} - 2\varphi^n_{i,j} + \varphi^n_{i,j-1}}{\Delta z^2}.$$

Divergence operator diagram

$$(\nabla \cdot \mathbf{u})^n_{i,j} = \frac{1}{r_i}\frac{r_{i+\frac{1}{2}} u^n_{r,i+\frac{1}{2},j} - r_{i-\frac{1}{2}} u^n_{r,i-\frac{1}{2},j}}{\Delta r} + \frac{u^n_{z,i,j+\frac{1}{2}} - u^n_{z,i,j-\frac{1}{2}}}{\Delta z},$$

$$u^n_{z,i,j+\frac{1}{2}} = \frac{u^n_{z,i,j+1} + u^n_{z,i,j}}{2}.$$

The discrete Kozeny-Carman formula is introduced as follows:

$$\varkappa^n_{i,j} = \frac{\left(\varepsilon^n_{i,j}\right)^3 d_f^2}{180\left(1 - \varepsilon^n_{i,j}\right)^2}.$$

Equations for hydraulics (Brinkman–Darcy+ projection) are introduced as follows:

"Darcy step" (velocity determination by pressure gradient) discrete values

$$u^{n+\frac{1}{2}}_{r,i,j} = -\frac{\varkappa^n_{i,j}}{\mu}(\partial_r p)^n_{i,j},$$
$$u^{n+\frac{1}{2}}_{z,i,j} = -\frac{\varkappa^n_{i,j}}{\mu}(\partial_z p)^n_{i,j}.$$

Brinkman diffusion/resistance correction (explicit) schemes

$$u_{r,i,j}^{n+1} = u_{r,i,j}^{n+\frac{1}{2}} + \Delta t \left[\frac{\mu}{\rho} (\nabla^2 u_r)_{i,j}^n - \frac{\mu}{\rho \varkappa_{i,j}^n} u_{r,i,j}^n \right],$$

$$u_{z,i,j}^{n+1} = u_{z,i,j}^{n+\frac{1}{2}} + \Delta t \left[\frac{\mu}{\rho} (\nabla^2 u_z)_{i,j}^n - \frac{\mu}{\rho \varkappa_{i,j}^n} u_{z,i,j}^n \right],$$

Projection equations (to enhance compression) are introduced as follows.

Determination of pressure renewal in the Poisson operator

$$(\nabla^2 p)_{i,j}^{n+1} = \frac{\rho}{\Delta t} (\nabla \cdot \mathbf{u})_{i,j}^{n+1}.$$

In practice, we can balance the velocity by performing this equation up to 3 times in Jacobi/GS relaxation steps

$$u_{r,i,j}^{n+1} \leftarrow u_{r,i,j}^{n+1} - \frac{\Delta t}{\rho} \left(\frac{\partial p}{\partial r} \right)_{i,j}^{n+1},$$

$$u_{z,i,j}^{n+1} \leftarrow u_{z,i,j}^{n+1} - \frac{\Delta t}{\rho} \left(\frac{\partial p}{\partial z} \right)_{i,j}^{n+1}.$$

The index range is defined as follows: for internal nodes $i = 1, \ldots, N_r - 1$, $j = 1, \ldots, N_z - 1$. For boundary values, the boundary conditions of Section 5 are applied.

Substance transport (ADR) is introduced for each component as follows:

Upwind convection flow detection schemes:

For the radial direction

$$c_{k,i+\frac{1}{2},j}^{n,\mathrm{up}} = \begin{cases} c_{k,i,j}^n, & u_{r,i+\frac{1}{2},j}^n > 0, \\ c_{k,i+1,j}^n, & u_{r,i+\frac{1}{2},j}^n \leqslant 0, \end{cases} \quad c_{k,i-\frac{1}{2},j}^{n,\mathrm{up}} = \begin{cases} c_{k,i-1,j}^n, & u_{r,i-\frac{1}{2},j}^n > 0, \\ c_{k,i,j}^n, & u_{r,i-\frac{1}{2},j}^n \leqslant 0, \end{cases}$$

$$(\mathcal{C}_r)_{i,j}^n = \frac{1}{r_i} \frac{r_{i+\frac{1}{2}} u_{r,i+\frac{1}{2},j}^n c_{k,i+\frac{1}{2},j}^{n,\mathrm{up}} - r_{i-\frac{1}{2}} u_{r,i-\frac{1}{2},j}^n c_{k,i-\frac{1}{2},j}^{n,\mathrm{up}}}{\Delta r}.$$

For axial direction

$$c_{k,i,j+\frac{1}{2}}^{n,\mathrm{up}} = \begin{cases} c_{k,i,j}^n, & u_{z,i,j+\frac{1}{2}}^n > 0, \\ c_{k,i,j+1}^n, & u_{z,i,j+\frac{1}{2}}^n \leqslant 0, \end{cases} \quad c_{k,i,j-\frac{1}{2}}^{n,\mathrm{up}} = \begin{cases} c_{k,i,j-1}^n, & u_{z,i,j-\frac{1}{2}}^n > 0, \\ c_{k,i,j}^n, & u_{z,i,j-\frac{1}{2}}^n \leqslant 0, \end{cases}$$

$$(\mathcal{C}_z)_{i,j}^n = \frac{u_{z,i,j+\frac{1}{2}}^n c_{k,i,j+\frac{1}{2}}^{n,\mathrm{up}} - u_{z,i,j-\frac{1}{2}}^n c_{k,i,j-\frac{1}{2}}^{n,\mathrm{up}}}{\Delta z}.$$

Schemes for diffusion (central, effective)

$$(\mathcal{D})_{i,j}^n = \frac{1}{r_i} \frac{r_{i+\frac{1}{2}} \varepsilon_{i+\frac{1}{2},j}^n D_{k,eff}^n \left(c_{k,i+1,j}^n - c_{k,i,j}^n \right) - r_{i-\frac{1}{2}} \varepsilon_{i-\frac{1}{2},j}^n D_{k,eff}^n \left(c_{k,i,j}^n - c_{k,i-1,j}^n \right)}{\Delta r^2} +$$
$$+ \varepsilon_{i,j}^n D_{k,eff}^n \frac{c_{k,i,j+1}^n - 2c_{k,i,j}^n + c_{k,i,j-1}^n}{\Delta z^2},$$

where

$$\varepsilon_{i\pm\frac{1}{2},j}^n = \frac{\varepsilon_{i\pm1,j}^n + \varepsilon_{i,j}^n}{2}.$$

Sources (reaction/adsorption) equations in explicit schema

$$R^n_{k,i,j} = -r^n_{k,\text{bulk},i,j} - a_s r^n_{k,\text{surf},i,j}.$$

Conservative form (with pores) schemes

$$W = \varepsilon c_k$$
$$W^{n+1}_{i,j} = W^n_{i,j} - \Delta t \left[(\mathcal{C}_r)^n_{i,j} + (\mathcal{C}_z)^n_{i,j}\right] + \Delta t(\mathcal{D})^n_{i,j} + \Delta t R^n_{k,i,j}.$$

Updated by $c^{n+1}_{k,i,j} = \frac{W^{n+1}_{i,j}}{\varepsilon^{n+1}_{i,j}}$ (ε^{n+1} determined in the following schemes).
Schemes for adsorption (LDF) and Langmuir isotherm:
Schematic representation for Langmuir equilibrium

$$q^{*,n}_{k,i,j} = \frac{q_{k,\max} b_k c^n_{k,i,j}}{1 + \sum_{m=1}^{N} b_m c^n_{m,i,j}}.$$

Schematic representation for LDF kinetics (explicit)

$$q^{n+1}_{k,i,j} = q^n_{k,i,j} + \Delta t k_{f,k} \left(q^{*,n}_{k,i,j} - q^n_{k,i,j}\right).$$

Schematic view for surface source

$$r^n_{k,\text{surf},i,j} = \rho_s \frac{q^{n+1}_{k,i,j} - q^n_{k,i,j}}{\Delta t}.$$

Schemes for particle clogging and porosity are determined as follows.
ADR schema for particles:

$$(\varepsilon c_p)^{n+1}_{i,j} = (\varepsilon c_p)^n_{i,j} - \Delta t \left[(\mathcal{C}^{(p)}_r)^n_{i,j} + (\mathcal{C}^{(p)}_z)^n_{i,j}\right] + \Delta t(\mathcal{D}_p)^n_{i,j} - \Delta t k_{\text{dep}} c^n_{p,i,j},$$

Where $\left(\mathcal{C}^{(p)}_r\right), \left(\mathcal{C}^{(p)}_z\right), (\mathcal{D}_p)$ is determined by the formulas in part 4 and using c_p and $D_{p,eff}$.
Porosity renewal scheme:

$$\varepsilon^{n+1}_{i,j} = \varepsilon^n_{i,j} - \Delta t \frac{\nu_{\text{dep}}}{\rho_{\text{dep}}} k_{\text{dep}} c^n_{p,i,j},$$

$$\varkappa^{n+1}_{i,j} = \varkappa\left(\varepsilon^{n+1}_{i,j}\right).$$

Determination of the membrane diagram (if it is present $j = N_z$ at the output):
Volumetric flow density diagram,

$$J^n_{v,i} = \frac{\Delta P}{\mu\left(R_m + R^n_{c,i}\right)}, R^n_{c,i} = \alpha_c \delta^n_{c,i}.$$

Flow balance for each component (for normal $+\hat{z}$):

$$-\varepsilon^n_{i,N_z} D^n_{k,eff} \frac{c^n_{k,i,N_z} - c^n_{k,i,N_z-1}}{\Delta z} + c^n_{k,i,N_z} J^n_{v,i} = J^n_{k,i},$$

where $J^n_{k,i}$ — the flow of matter through the membrane (depending on your model, for example $J_k = P_k\left(c_{\text{up}} - c_{\text{down}}\right)$).

Colmatation thickness over the membrane:

$$\delta_{c,i}^{n+1} = \delta_{c,i}^{n} + \Delta t \frac{J_{v,i}^{n} c_{p,m,i}^{n}}{\rho_c},$$

Where $c_{p,m,i}^{n}$ – concentration of particles on the membrane surface (usually $j = N_z$ or the value of the adjacent cell).

The schemes of boundary and initial conditions are determined as follows:

Initial conditions (for all i, j):

$$p_{i,j}^{0} = p_0\left(r_i, z_j\right), \;\; u_{r,i,j}^{0} = u_{r0}\left(r_i, z_j\right),$$
$$u_{z,i,j}^{0} = u_{z0}\left(r_i, z_j\right),$$

$$c_{k,i,j}^{0} = c_{k0}\left(r_i, z_j\right), \;\; q_{k,i,j}^{0} = q_{k0}\left(r_i, \;\; z_j\right),$$
$$c_{p,i,j}^{0} = c_{p0}\left(r_i, z_j\right), \;\; \varepsilon_{i,j}^{0} = \varepsilon_0\left(r_i, z_j\right), \;\; \delta_{c,i}^{0} = \delta_{c0}\left(r_i\right).$$

Schemes for inlet $z = 0$ (i.e. $j = 0$).

Pressure and speed condition:

$$p_{i,0}^{n} = p_{\text{in}}\left(t^n\right), \;\; u_{z,i,\frac{1}{2}}^{n} = u_{\text{in}}\left(t^n\right).$$

Scheme for determining concentrations (according to Dirichlet):

$$c_{k,i,0}^{n} = c_{k,\text{in}}\left(t^n\right), \;\; c_{p,i,0}^{n} = c_{p,\text{in}}\left(t^n\right).$$

If the velocity is given, the pressure gradient is matched with the central/boundary difference at the input.

Schemes for outlet: $z = H$ (i.e. $j = N_z$)

For pressure:

$$p_{i,N_z}^{n} = p_{\text{out}}\left(\approx p_{\text{atm}}\right).$$

Zero gradient (Neumann) or convective output if there is no membrane:

$$\frac{c_{k,i,N_z}^{n} - c_{k,i,N_z-1}^{n}}{\Delta z} = 0 \text{ or}$$
$$-\varepsilon D_{k,eff} \frac{c_{k,i,N_z}^{n} - c_{k,i,N_z-1}^{n}}{\Delta z} + c_{k,i,N_z}^{n} u_{z,i,N_z-\frac{1}{2}}^{n} = 0.$$

If the membrane is present, the flow balance and refresh δ_c in Part 7 is applied.

Schemes for the side wall: $r = R$ (i.e. $i = N_r$)

Diagrams for radial and symmetrical axil directions:

$$u_{r,N_r,j}^{n} = 0, \;\; \frac{u_{z,N_r,j}^{n} - u_{z,N_r-1,j}^{n}}{\Delta r} = 0.$$

Zero flow for diffusion

$$\frac{c_{k,N_r,j}^{n} - c_{k,N_r-1,j}^{n}}{\Delta r} = 0,$$
$$\frac{c_{p,N_r,j}^{n} - c_{p,N_r-1,j}^{n}}{\Delta r} = 0.$$

On symmetric axes: $r = 0$ (i.e. $i = 0$):

$$u^n_{r,0,j} = 0, \quad \frac{u^n_{z,1,j} - u^n_{z,0,j}}{\Delta r} = 0,$$
$$\frac{c^n_{k,1,j} - c^n_{k,0,j}}{\Delta r} = 0, \quad \frac{c^n_{p,1,j} - c^n_{p,0,j}}{\Delta r} = 0.$$

Approaches $\frac{\partial^2\varphi}{\partial r^2}$ the limit $\frac{1}{r}\frac{\partial\varphi}{\partial r}$ at; in effect:

$$(\nabla^2\varphi)^n_{0,j} \approx \frac{2\left(\varphi^n_{1,j} - \varphi^n_{0,j}\right)}{\Delta r^2} + \frac{\varphi^n_{0,j+1} - 2\varphi^n_{0,j} + \varphi^n_{0,j-1}}{\Delta z^2}.$$

Complete order of the time step (index range) sequence of actions performed. At each time step:

(a) $\varkappa^n_{i,j} = \varkappa\left(\varepsilon^n_{i,j}\right)$ is calculated for all of $0 \leqslant i \leqslant N_r, 0 \leqslant j \leqslant N_z$.

(b) Darcy step $u^{n+\frac{1}{2}}_{r,i,j}, u^{n+\frac{1}{2}}_{z,i,j}$ is found at

$$i = 1..N_r - 1, j = 1..N_z - 1.$$

(c) Brinkman adjustment: $u^{n+1}_{r,i,j}, u^{n+1}_{z,i,j}$ will be updated explicitly in $i = 1..N_r - 1, j = = 1..N_z - 1$.

(d) Projection (for arbitrary 1-3 relexation): $p^{n+1}_{i,j}$ (in internal nodes), then u^{n+1} corrected with a gradient.

(e) For each k: $q^{n+1}_{k,i,j}$ will be updated with LDF(all nodes). $(\varepsilon c_k)^{n+1}_{i,j}$ update in internal nodes, then apply to the boundary conditions. If determined $c^{n+1}_{k,i,j} = (\varepsilon c_k)^{n+1}_{i,j}/\varepsilon^{n+1}_{i,j}$ is applied.

(f) By particle: $(\varepsilon c_p)^{n+1}_{i,j}$ is updated in internal nodes, then applied in boundary conditions: $\varepsilon^{n+1}_{i,j} = \varepsilon^n_{i,j} - \Delta t\left(\nu_{\text{dep}}/\rho_{\text{dep}}\right) k_{\text{dep}} c^n_{p,i,j}$, and then $\varkappa^{n+1}_{i,j}$ is recalculated.

(g) If there is a membrane ($j = N_z$):$J^n_{v,i}$, $J^n_{k,i}$ the flux conditions with and $\delta^{n+1}_{c,i}$ are applied.

(h) All boundary conditions are applied as in Section 8.

CFL(Courant-Friedrichs-Lewy) condition for stability:

$$\Delta t \leqslant \min\left\{\frac{\Delta r}{\max|u_r|}, \frac{\Delta z}{\max|u_z|}, \frac{1}{2}(D^{\max}_{eff}\left(\frac{1}{\Delta r^2} + \frac{1}{\Delta z^2}\right))^{-1}, \frac{\rho\varkappa_{\min}}{\mu}, \frac{1}{k_{f,\max}}, \frac{\rho_{\text{dep}}}{\nu_{\text{dep}} k_{\text{dep}} c_{p,\max}}\right\}.$$

4 Results and discussion

The results show the time-dependent behavior of membrane contamination, concentration polarization, increase in osmotic pressure, and decrease in flow, indicating that adsorption and particle deposition significantly reduce filtration efficiency over time.

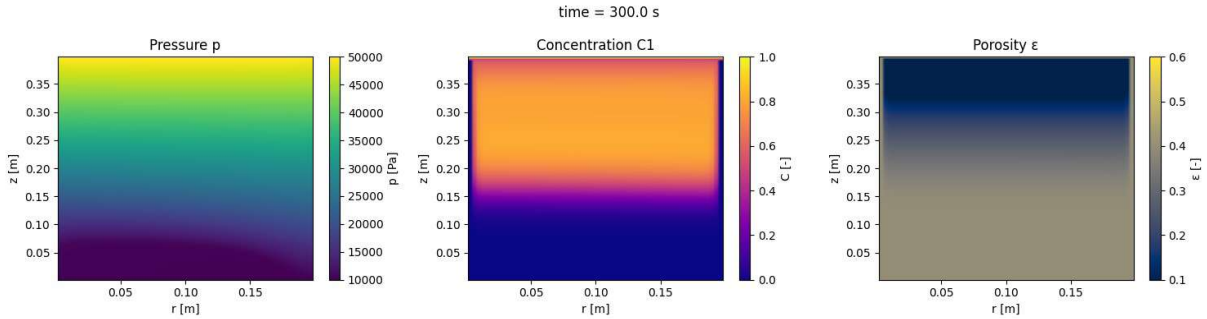

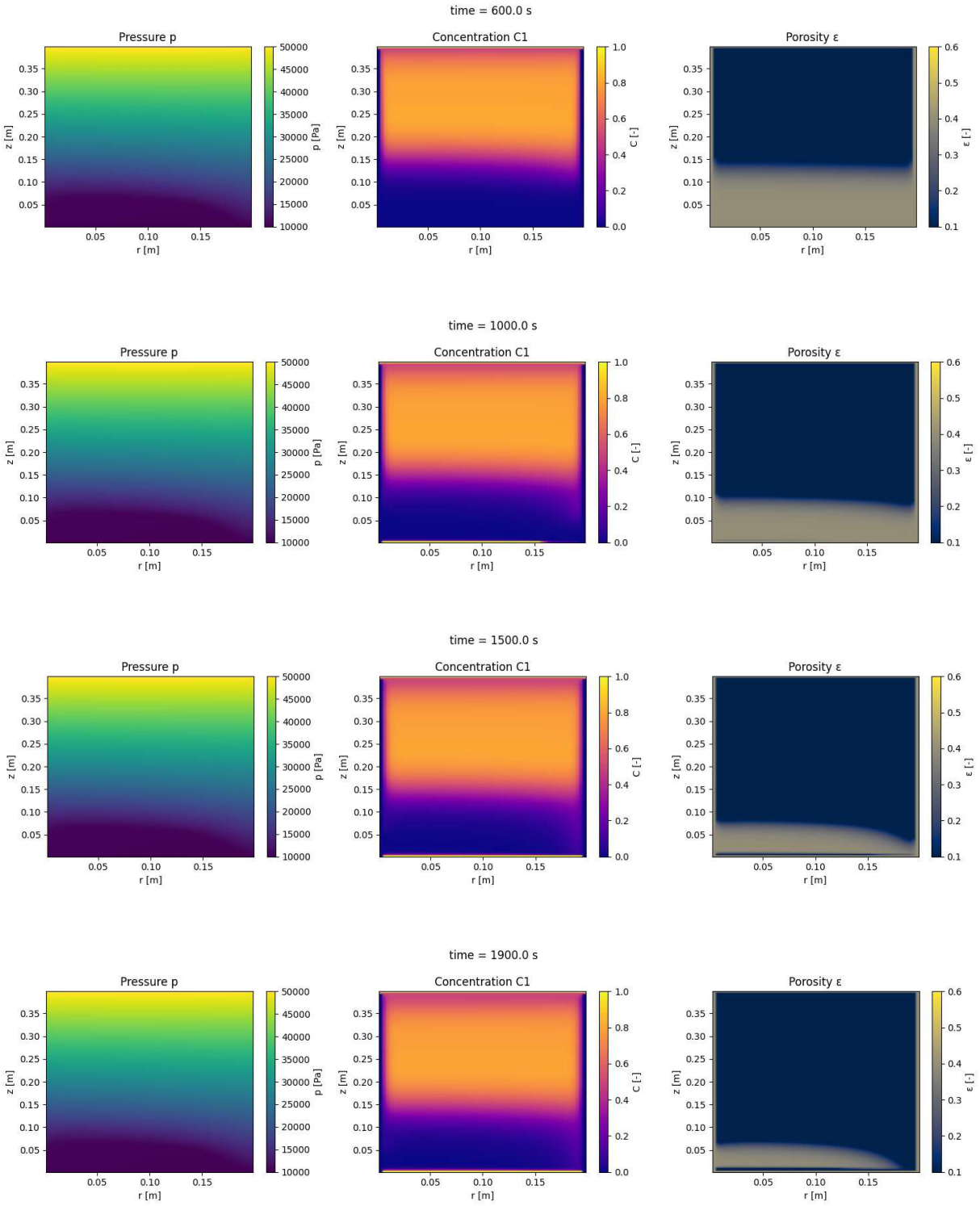

Figure 1 Changes in pressure distribution, solute concentration, and porosity over time in a porous filtration medium

The figures in figure 1 show the course of filtration and membrane contamination over time, highlighting the main stages of the process. In the early stages the dissolved substance is primarily transported downward by convection, and only a thin layer of contamination begins to develop near the membrane surface. By $t \approx 600\,s$, the accumulation of solute in the membrane becomes more pronounced, which indicates the beginning of a significant decrease in porosity. In intermediate stages a fully developed cake layer appears

and begins to move upward, toward the filter, significantly altering the concentration gradient. Later the contamination layer continues to thicken and gradually stabilizes, leading to a quasi-stable state where transport, adsorption, and membrane resistance reach equilibrium. At all stages, the pressure field remains predominantly linear, although small deviations near the membrane indicate an increase in hydraulic resistance due to the impact of contamination.

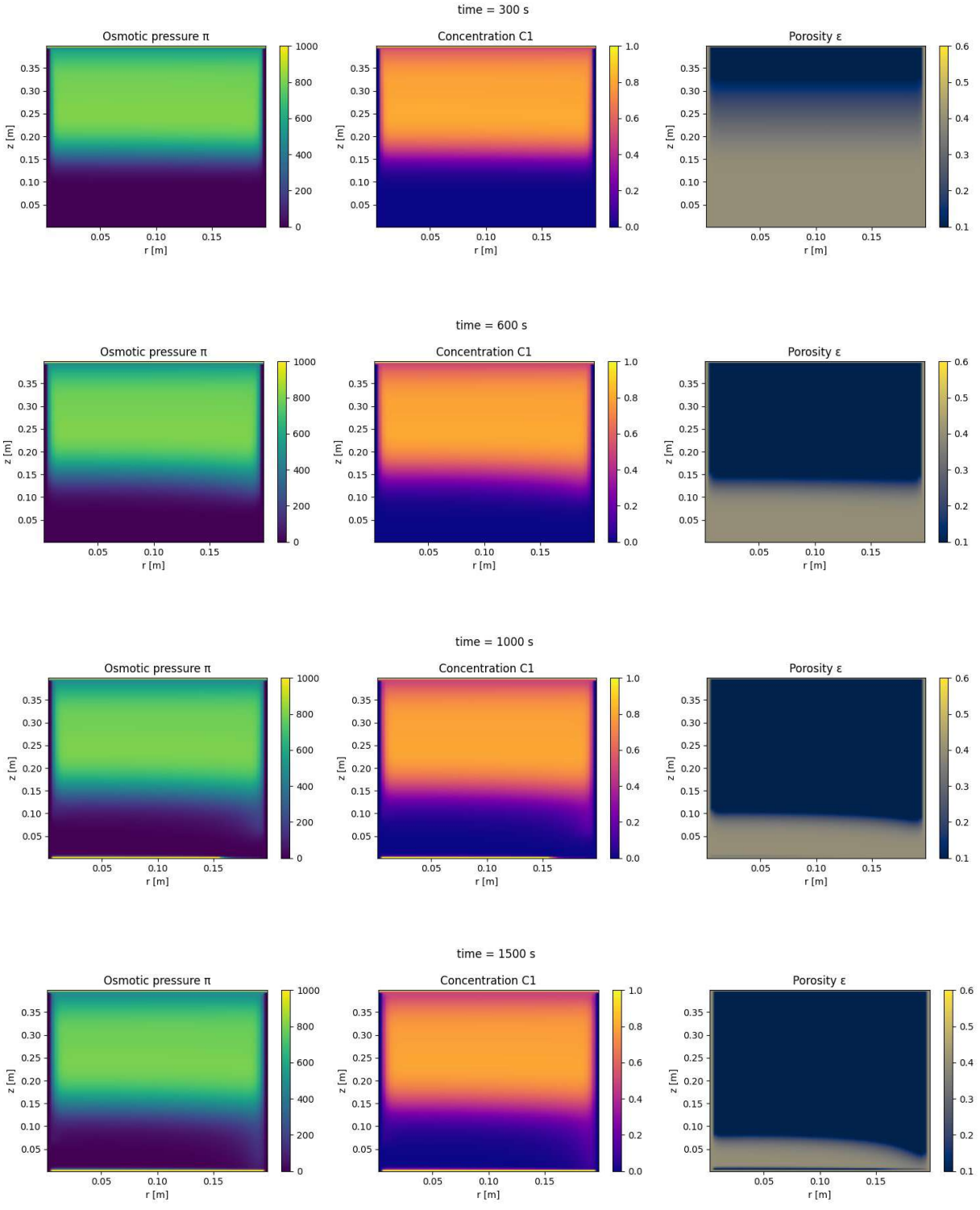

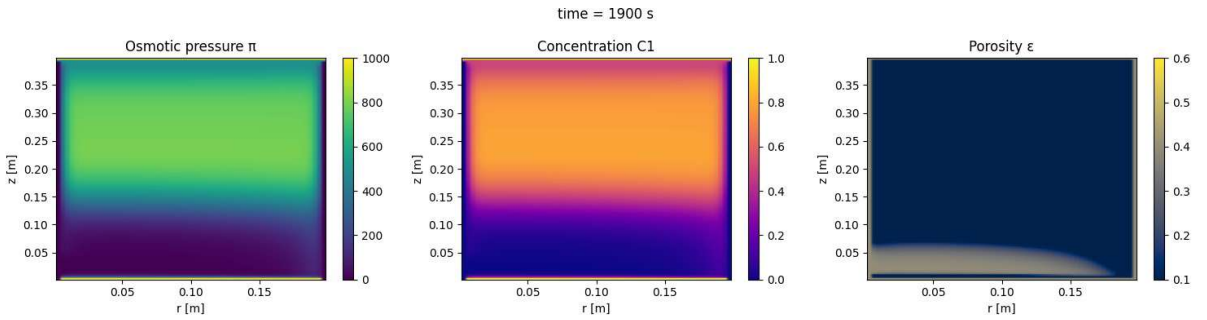

Figure 2 Temporary analysis of osmotic pressure, solute concentration, and porosity during membrane filtration

The figures show how membrane filtration changes over time, highlighting the interaction between osmotic pressure, solute concentration, and porosity over time ranging from 300 to 1900 seconds. At the initial stage, the dissolved substance moves downward and begins to accumulate near the membrane surface, leading to a slight increase in osmotic pressure and the early development of a thin layer of contamination with a slight decrease in porosity. Concentration polarization increases over time, leading to a significant increase in osmotic pressure near the membrane. This increases flow resistance and accelerates the formation of contamination, which appears as an expanding region with reduced porosity. In the subsequent stages, a fully developed cake layer appears and gradually grows upward in the filter. During this period, osmotic pressure approaches a nearly stable state, and the concentration distribution becomes more stable, indicating an equilibrium between the processes of convection, diffusion, and membrane removal. Overall, the results reveal the underlying mechanism of filtration: increased accumulation of dissolved matter increases osmotic pressure, which reduces the effective driving force and promotes continuous contamination until the system transitions to a quasi-stable state.

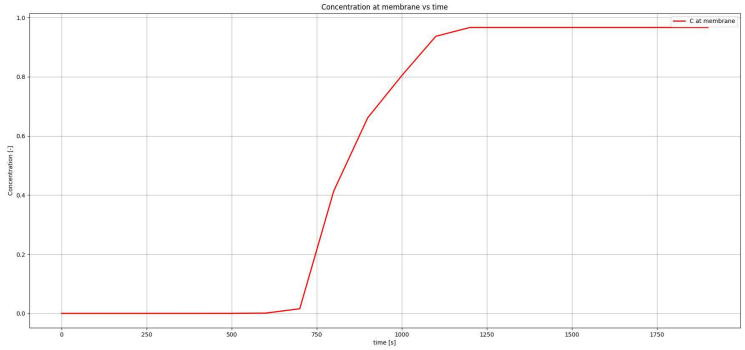

Figure 3 Evolution of solute concentration at the membrane surface over time

The graph shows how the concentration of the solute on the membrane surface changes over time, highlighting the development of concentration polarization. In the early stages , the concentration is almost zero, indicating that the solute front has not yet reached the membrane boundary. Rapid growth occurs around $t \approx 700-900\,s$, which is determined by the arrival of the solute front and the onset of significant accumulation on the membrane surface. Subsequently ($t > 1000\,s$), the concentration ceases and approaches a plateau near the inlet concentration, indicating saturation and the formation of a quasi-stable state governed by an equilibrium between convection, diffusion, and membrane rejection effects.

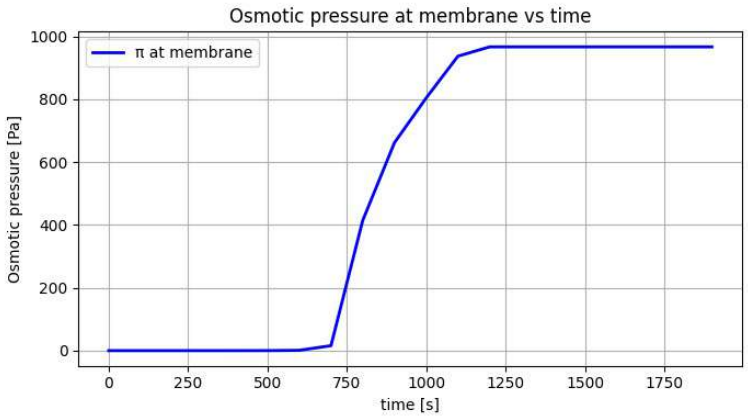

Figure 4 Evolution of osmotic pressure at the membrane surface over time

The graph shows how the osmotic pressure on the membrane surface changes over time, reflecting the development of concentration polarization. In the initial stage, osmotic pressure is almost zero, indicating that the solute has not yet reached the membrane. In the range of approximately $t \approx 700\breve{}1000\,s$, a sharp rise occurs as a result of the accumulation of dissolved matter at the membrane boundary, leading to a significant increase in osmotic resistance. In the subsequent period ($t > 1100\,s$), the curve smooths out, indicating the formation of a quasi-stable state in which the saturation and transport processes reach equilibrium.

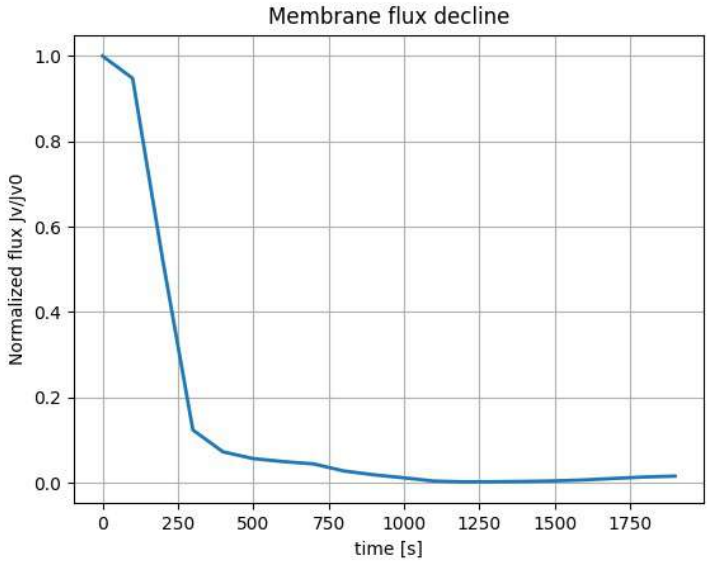

Figure 5 Evolution of normalized flux at the membrane surface over time

The graph shows how normalized membrane flow decreases over time as a result of pollution. In the initial period, the flow is close to its initial level, indicating that the membrane is still pure and shows little resistance to the flow. Approximately within the range of $t \approx 100 - 300\,s$, a pronounced decrease occurs, indicating the onset of contamination and rapid pore clogging. In subsequent stages ($t > 1000\,s$), the flow decreases toward near-zero values and then stabilizes, indicating the development of a compact contamination layer and the establishment of a quasi-stable state in which membrane resistance predominates.

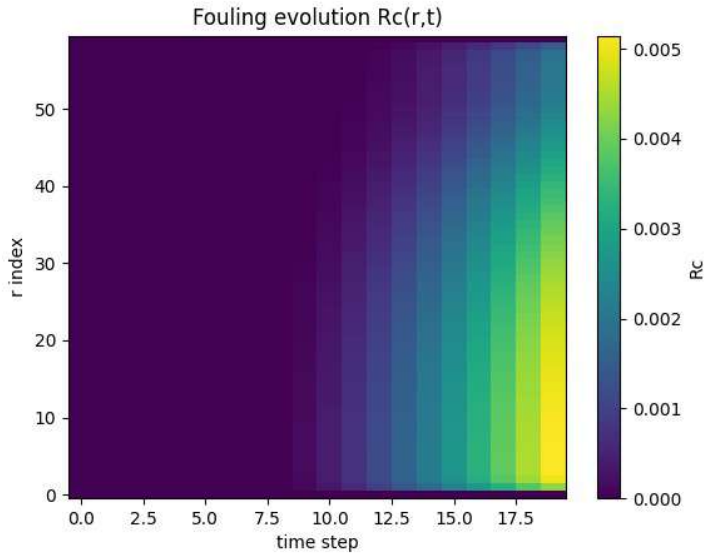

Figure 6 Evolution of membrane fouling at the membrane surface over time

The figure shows the temporal and radial evolution of membrane contamination resistance $R_c(t)$. Initially, contamination along the entire radius is insignificant, indicating the cleanliness of the membrane. Over time (t ≈ 10–20 steps), pollution develops rapidly and increases especially near the center of high flow intensity (r ≈ 0). The radial gradient indicates that pollution is not uniform, is more concentrated in the central region, and settles more weakly than at the edges. Overall, the graph highlights the progressive accumulation of cake resistance over time and its spatial heterogeneity, leading to a decrease in membrane properties.

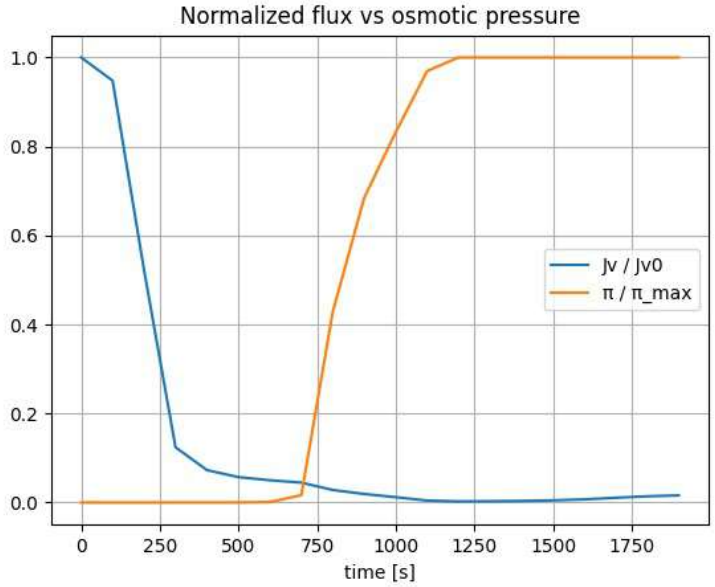

Figure 7 Normalized flux and osmotic pressure change over time

The graph shows the relationship between normalized membrane flow and osmotic pressure, highlighting their inverse relationship during filtration. Initially, the flow rate

is high, and osmotic pressure is insignificant, indicating minimal resistance. As filtration progresses ($t \approx 700 - 1000\,s$), osmotic pressure increases rapidly due to the accumulation of solute in the membrane, and the flux decreases sharply. Recently, osmotic pressure has reached a plateau, and the flow approaches values close to zero, indicating the establishment of a polluted, transport-limited regime. Overall, the graph clearly shows that an increase in osmotic pressure is the primary factor leading to a decrease in flow.

5 Conclusion

In this study, a bound numerical system was developed and implemented using the finite volume method to model the filtration flow and transport of dissolved substances in a cylindrical porous filter. The flow dynamics are governed by the axially symmetrical Brinkman-Darcy equations, while the transport of dissolved substances is described by the advection-diffusion equations, which include the kinetics of adsorption. The relationship between conductivity and porosity is determined using the Kozeny-Carman equation, which allows for a consistent description of the developing porous structure in the model.

The modeling results provide a physically coherent distribution of pressure, concentration, and porosity, confirming the stability and preservation properties of the finite volume scheme. The results show that filtration is primarily ensured by the axial pressure gradient, while the transport of dissolved substances is influenced by the effects of convection, diffusion, and adsorption. Over time, adsorption and particle accumulation reduce porosity, leading to a decrease in permeability and a decrease in filtration rates. These results highlight a strong correlation between fluid flow, mass transfer, adsorption, and structural changes in the porous medium. The model successfully reflects the transient process of filter saturation and worsening performance, which is important for evaluating the service life and operational efficiency of the filter.

Overall, the proposed method offers a reliable and flexible computational system for studying filtration and transport phenomena in cylindrical porous systems. It can be further refined by introducing more advanced reaction mechanisms, non-Darcy flow behavior, or experimental validation, making it suitable for designing and optimizing the filtration system.

References

[1] Ravshanov N., Boborahimov B.I., Berdiyorov Sh.Sh. *Numerical modeling of liquid solution filtration in a cylindrical porous filter // Problems of Computational and Applied Mathematics.* – 2025. – № 5(69). doi: http://dx.doi.org/10.71310/pcam.5_69.2025.04.

[2] Ravshanov N., Boborahimov B.I., Berdiyorov Sh.Sh. *Numerical modeling of filtration and transport processes in a cylindrical porous filter using the finite volume method // Problems of Computational and Applied Mathematics.* – 2026. – № 1(71). doi: http://dx.doi.org/10.71310/pcam.1_71.2026.03.

[3] Ravshanov N., Abdullaev Z., Khafizov O. *Modeling the filtration of groundwater in multilayer porous media // Construction of Unique Buildings and Structures.* – 2020. – Vol. 92. – Art. 9206.

[4] Ravshanov N., Turakulov J., Turkmanova S., Ungalov S. *Numerical study of technological process of liquid solution filtration // AIP Conference Proceedings.* – 2025. – Vol. 3256. – Art. 040017. doi: http://dx.doi.org/10.1063/5.0267147.

[5] Kalandarbekov I., Smuleac L., Jurakhonzoda R., Rasulov U. *Mathematical model construction of the isotropic filtration process based on Darcy's law // Research Journal of Agricultural Science.* – 2022. – Vol. 54(1). – P. 90–95.

[6] Karimova I.M., Turdiev T.T. *Problems and major problems of mathematical modeling of fluid motion in non-homogeneous media* // *The American Journal of Engineering and Technology*. – 2021. – Vol. 3(2). – P. 83–89. doi: http://dx.doi.org/10.37547/tajet/Volume03Issue02-12

[7] Gizzatullina A. *Mathematical modeling of filtration flows in hydraulic fracturing cracks* // *Socar Proceedings*. – 2024. – № 4. – P. 72–78.

[8] Kayumov S., Arzikulov G., Bekchanov S., Zuyadullayeva S. *A multiparameter mathematical model for nonlinear filtration in two-layer media* // *Journal of Physics: Conference Series*. – 2024. – Vol. 2697. – Art. 012042. doi: http://dx.doi.org/10.1088/1742-6596/2697/1/012042

[9] Kayumov Sh., Arzikulov G.P., Bekchanov Sh.E., Khusanov E.A. *Mathematical models of fluid filtration in a three-layer medium* // *Vestnik Osh State University*. – 2024. – № 1(4).

[10] Kayumov Sh., Mardanov A.P., Tuychieva S.T., Kayumov A.B. *Mathematical modeling of structured and Newtonian fluids in associated layers* // *E3S Web of Conferences*. – 2023. – Vol. 401. – Art. 01086. doi: http://dx.doi.org/10.1051/e3sconf/202340101086

[11] Seyfi H., Shafiei S., Dehghanzadeh R., Amirabedi P. *Mathematical modeling and optimization of acrylonitrile degradation in biofilters* // *Iranian Journal of Chemical Engineering*. – 2021. – Vol. 18(3). – P. 3–15.

[12] Khuzhayorov B., Djiyanov T.O., Zokirov M.S. *Generalized fractional differential model of fluid filtration in porous media* // *International Journal of Applied Mathematics*. – 2024. – Vol. 37(1). – P. 119–132. doi: http://dx.doi.org/10.12732/ijam.v37i1.10

[13] Makhmudov J.M., Usmonov A.I., Kuljanov J.B. *Anomalous filtration in nonhomogeneous porous media* // *International Journal of Applied Mathematics*. – 2023. – Vol. 36(2). – P. 189–203. doi: http://dx.doi.org/10.12732/ijam.v36i2.4

[14] Koka R., Ganjikunta A. *Effect of the Aligned Magnetic Field Over a Stretching Sheet Through Porous Media in Casson Fluid Flow* // *CFD Letters*. – 2024. – Vol. 16. – № 4. – P. 16–38. doi: http://dx.doi.org/10.37934/cfdl.16.4.1638

[15] Vecherkovskaya A., Popereshnyak S. *Mathematical modeling of fluid filtration through multilayer filtering element* // *Technology Audit and Production Reserves*. – 2017. – Vol. 4. – № 3(36). – P. 9–13. doi: http://dx.doi.org/10.15587/2312-8372.2017.109309

УДК 519.6+51-74::628.395

ХАРАКТЕРИСТИКИ ЗАГРЯЗНЕНИЯ МЕМБРАНЫ В ПРОЦЕССЕ ФИЛЬТРАЦИИ И ТРАНСПОРТИРОВКИ В ЦИЛИНДРИЧЕСКОМ ПОРИСТОМ ФИЛЬТРЕ

Равшанов Н., Боборахимов Б.И., *Бердиёров Ш.Ш.

*berdiyorovsh@gmail.com

Научно-исследовательский институт развития цифровых технологий и искусственного интеллекта,

100125, Узбекистан, г. Ташкент, Мирзо-Улугбекский р-он, м-в Буз-2, д. 17А.

В данном исследовании представлена математическая и численная модель фильтрации, переноса растворенных веществ, адсорбции и загрязнения мембраны в цилиндрическом пористом фильтре. Модель сочетает осесимметричные уравнения потока Бринкмана–Дарси с уравнениями адвекции–диффузии–реакции, адсорбцией

Лангмюра и моделью линейной движущей силы (ЛДС). Также учитываются изменения пористости, осаждение частиц, образование осадка, осмотическое давление и рост сопротивления мембраны. Для моделирования используется конечно-разностная схема с управлением устойчивостью на основе КФЛ. Результаты показывают, что адсорбция и осаждение частиц значительно снижают пористость и проницаемость мембраны, что приводит к увеличению гидравлического сопротивления и снижению потока. Модель предоставляет полезную основу для прогнозирования динамики загрязнения и оптимизации пористых фильтрационных систем.

Ключевые слова: цилиндрический пористый фильтр, загрязнение мембраны, модель Бринкмана–Дарси, уравнения адвекции–диффузии–реакции, кинетика адсорбции, изотерма Лангмюра, концентрационная поляризация, осмотическое давление, образование осадочного слоя, перенос в пористых средах, метод конечных разностей, процессы фильтрации.

Цитирование: *Равшанов Н., Боборахимов Б.И., Бердиёров Ш.Ш.* Характеристики загрязнения мембраны в процессе фильтрации и транспортировки в цилиндрическом пористом фильтре // Проблемы вычислительной и прикладной математики. – 2026. – № 3(73). – С. 104-124.

DOI: https://doi.org/10.71310/pcam.3_73.2026.08

№ 3(73) 2026

ISSN 2181-8460

HISOBLASH VA AMALIY MATEMATIKA MUAMMOLARI

ПРОБЛЕМЫ ВЫЧИСЛИТЕЛЬНОЙ И ПРИКЛАДНОЙ МАТЕМАТИКИ

PROBLEMS OF COMPUTATIONAL AND APPLIED MATHEMATICS

AiRI
RAQAMLI TEXNOLOGIYALAR VA SUN'IY INTELLEKTNI RIVOJLANTIRISH ILMIY-TADQIQOT INSTITUTI

ПРОБЛЕМЫ ВЫЧИСЛИТЕЛЬНОЙ И ПРИКЛАДНОЙ МАТЕМАТИКИ

№ 3(73) 2026

Журнал основан в 2015 году.
Издается 6 раз в год.

Учредитель:
Научно-исследовательский институт развития цифровых технологий и искусственного интеллекта.

Журнал зарегистрирован в Агентстве информации и массовых коммуникаций при Администрации Президента Республики Узбекистан.
Свидетельство №0856 от 5 августа 2015 года.

ISSN 2181-8460, eISSN 2181-046X

Адрес редакции:
100125, г. Ташкент, м-в. Буз-2, 17А.
Тел.: +(998) 71 263-41-98.
Э-почта: journals@airi.uz.
Веб-сайт: https://journals.airi.uz.

Дизайн и вёрстка:
Шарипов Х.Д.

Отпечатано в типографии НИИ РЦТИИ.
Подписано в печать 25.06.2026 г.
Формат 60x84 1/8. Заказ №3. Тираж 100 экз.

PROBLEMS OF COMPUTATIONAL AND APPLIED MATHEMATICS

No. 3(73) 2026

The journal was established in 2015.
6 issues are published per year.

Founder:
Digital Technologies and Artificial Intelligence Development Research Institute.

The journal is registered by Agency of Information and Mass Communications under the Administration of the President of the Republic of Uzbekistan.
Certificate of Registration No. 0856 of 5 August 2015.

ISSN 2181-8460, eISSN 2181-046X

Address:
100125, Tashkent, Buz-2, 17A.
Tel.: +(998) 71 263-41-98.
E-mail: journals@airi.uz.
Web-site: https://journals.airi.uz.

Layout design:
Sharipov Kh.D.

DTAIRI printing office.
Signed for print 25.06.2026
Format 60x84 1/8. Order No. 3. Print run of 100 copies.

Содержание

Яхшибаев Д.С., Боборахимов Б.И.
Математическое моделирование поступления многофазного потока смеси в стратифицированное водохранилище и разрушения слоистой структуры . . . 7

Бахтиёров Б.Б., Хужаев И.К., Туропова Н.В.
Математическая модель и анализ гашения гидравлического удара с помощью воздушного колпака 25

Бегимов О.М., Хужаев И.К., Мамадалиев Х.А.
Исследование скорости распространения малых возмущений давления в газожидкостной среде с учетом массовой концентрации газа и деформации стенки трубопровода 37

Эргашев Д.Й., Хужаев Ж.И., Ахмаджонов С.С.
Математическая модель процесса теплоотдачи от жидкого теплоносителя, текущего по оребренному прямоугольными ребрами цилиндрическому трубопроводу 50

Музаффаров С.А., Маратов Х.У., Хамдамов А.А.
Вычислительное моделирование вертикально-осевой ветроэнергетической установки с пассивным изменением шага лопастей для условий слабых ветров 61

Хожикулов Ш.Ш., Бегимов О.М., Обиджонов А.Ж.
Исследование динамики переходных процессов, связанных с изменением расхода в конце участка трубопровода, с учетом и без учета силы сопротивления 75

Равшанов Ш.А., Боборахимова М.И., Чуллиев Ш.И.
Моделирование тепло- и массообмена в рельефном трубопроводе с постоянными и изменяющимися диаметрами 90

Равшанов Н., Боборахимов Б.И., Бердиёров Ш.Ш.
Характеристики загрязнения мембраны в процессе фильтрации и транспортировки в цилиндрическом пористом фильтре 104

Халджигитов А.А., Бобоназаров А.А., Рахмонова Р.А., Тиловов О.О.
Численное моделирование задач теории упругости в напряжениях методом конечных элементов 125

Тиловов М.А.
Численное исследование динамики производных различного порядка уравнения Фолкнера–Скэна в зависимости от градиента давления 139

Жумаев З.З.
Приближённое решение задач с начальными условиями для дифференциальных уравнений первого порядка с использованием комбинированного метода Рунге–Кутты и метода с кусочно-постоянным аргументом 153

Contents

Yakhshibaev D.S., Boborakhimov B.I.
Mathematical modeling of multiphase mixture inflow into a stratified reservoir and the breakdown of the layered structure 7

Bakhtiyorov B.B., Khujaev I.K., Turapova N.V.
Mathematical model and analysis of water hammer damping using an air vessel . 25

Begimov O.M., Khujaev I.K., Mamadaliev Kh.A.
Investigation of the propagation velocity of small pressure disturbances in a gas–liquid medium with account for gas mass concentration and pipeline wall deformation 37

Ergashev D.Y., Khujaev J.I., Akhmadjonov S.S.
A mathematical model of heat transfer from a liquid coolant flowing through a cylindrical pipeline finned with rectangular fins 50

Muzaffarov S.A., Maratov Kh.U., Hamdamov M.M.
Computational modeling of a passive-pitch low-wind vertical-axis wind turbine . 61

Khozhikulov Sh.Sh., Begimov O.M., Obidjonov A.J.
Investigation into the dynamics of transient processes associated with flow rate changes at the end of a pipeline section, both with and without resistance force . 75

Ravshanov Sh.A., Boborakhimova M.I, Chulliev Sh.I.
Modelling heat and mass transfer in a relief pipeline with constant and varying diameters 90

Ravshanov N., Boborakhimov B.I., Berdiyorov Sh.Sh.
Membrane fouling characteristics during filtration and transport processes in a cylindrical porous filter 104

Khaldjigitov A.A., Bobonazarov A.A., Rakhmonova R.A., Tilovov O.O.
Numerical modeling of elasticity theory problems in terms of stresses using the finite element method 125

Tilovov M.A.
Numerical study of the dynamics of derivatives of various orders of the Falkner–Skan equation depending on the pressure gradient 139

Jumaev Z.Z.
Approximate solution of initial value problems for first-order differential equations using a combined Runge-Kutta and piecewise constant argument method . 153